Minimum-Voltage Vector Injection Method for Sensorless Control of PMSM for Low-Speed Operations

Ge Xie, Kaiyuan Lu, *Member, IEEE*, Sanjeet Kumar Dwivedi, *Senior Member, IEEE*, Jesper Riber Rosholm, and Frede Blaabjerg, *Fellow, IEEE*

***Abstract*—In this paper, a simple signal injection method is proposed for sensorless control of permanent-magnet synchronous machine (PMSM) at a low speed, which ideally requires one voltage vector only for position estimation. The proposed method is easy to implement, resulting in low computation burden. No filters are needed for extracting the high-frequency current signals for position estimation. The use of low-pass filters (LPFs) in the current control loop to obtain the fundamental current component is not necessary. Therefore, the control bandwidth of the inner current control loop may not need to be sacrificed. The proposed method may also be further developed to inject two opposite voltage vectors to reduce the effects of inverter voltage error on the position estimation accuracy. The effectiveness of the proposed method is demonstrated by comparing with other sensorless control method. Theoretical analysis and experimental results are given for validating the proposed new sensorless control method.**

***Index Terms*—Filter-free, high bandwidth, injection, inverter voltage error, low-speed range, permanent-magnet synchronous machine (PMSM), sensorless control, voltage.**

I. Introduction

PERMANENT-MAGNET synchronous machine (PMSM) has become the most promising drive motor candidate for many industrial applications due to its high efficiency and high torque density. Eliminating the mechanical sensor brings a lot advantages for the PMSM drive, i.e., lower cost, better reliability, and compactness in the drive system [1]. Therefore, sensorless control is increasingly used for various PMSM drive systems.

For medium- to high-speed operation, the method based on the fundamental model of the PMSM, also known as the back-EMF method, has been well established. Since the rotor north pole is fixed on the rotor *d*-axis, identifying the rotor flux location will give directly the rotor position [2]. A typical example utilizing the rotor *d*-axis flux is the active-flux concept [3], where a common *d*-axis flux model was proposed for various types of synchronous machines and used for position estimation. To obtain the flux, integration of the voltage is required, which needs to deal with dc offsets introduced by current sensors, stator phase resistance variation, and wrong integrator initial values. To avoid these problems, the back-EMF voltage may be directly used for positon estimation [4]. Various other issues regarding inductance variation treatment in back-EMF-based sensorless control and its performance with respect to measurement errors and inverter nonlinearities have been well studied in [5] and [6].

For low-speed operation, the position has to be estimated from the rotor saliency (the difference of the *d*-axis and *q*-axis inductances) and various high-frequency injection methods have been used. The high-frequency voltage could be injected on the estimated reference frames [7]–[9] or on the stationary reference frame [10]. Arbitrary injection seems also to be possible [11]. The injected voltage could be sinusoidal [7]–[10] or square wave [12]. Some comparative studies for different injection methods are given in [13]. During the starting, the initial rotor magnetic polarity needs to be identified. This is often done by injecting testing voltage pulses that will cause different magnetic saturation on the rotor positive and negative *d*-axis, respectively [9], [14].

For many of the existing high-frequency injection methods, filters are needed for: 1) extracting high-frequency current responses for position estimation; and 2) removing the high-frequency current ripples in the current control loop of the field-oriented controller (FOC), preventing the PI controllers from responding to the high-frequency current ripples. Use of filters will increase the complexity of the sensorless controller, and the current control loop filter may reduce the controller bandwidth and affect the total drive performance [12].

Roughly speaking, different injection methods may also be grouped by the way how the current differentiation in machine voltage equation is handled. The machine terminal voltage is controllable and is known. For sinusoidal high-frequency signal injection method, it normally assumes that the high-frequency signal is always in steady state. Therefore, the current differentiation will result in current phase angle shift and amplitude change. Another way to handle the current differentiation (di/dt) simply is to replace it with $\Delta i/\Delta t$, where Δt is typically less than or equal to one switching period. For example, in [14], the current variation is measured several times within one PWM period in order to form enough algebraic equations to solve for the rotor position. Current variation (Δi) measurement may also be executed during the zero-voltage vector period within one PWM period [15]. The main advantage of these methods is that they do not require special injection voltages. But the

Manuscript received December 17, 2014; revised February 24, 2015; accepted April 9, 2015. Date of publication April 24, 2015; date of current version September 29, 2015. Recommended for publication by Associate Editor J. Ojo.

G. Xie, K. Lu, and F. Blaabjerg are with the Department of Energy Technology, Aalborg University, Graasten 6300, Denmark (e-mail: gxi@et.aau.dk; klu@et.aau.dk; fbl@et.aau.dk).

S. K. Dwivedi and J. R. Rosholm are with Danfoss Power Electronics A/S, Graasten 6300, Denmark (e-mail: sanjeet@danfoss.com; riber@danfoss.com).

Color versions of one or more of the figures in this paper are available online at http://ieeexplore.ieee.org.

Digital Object Identifier 10.1109/TPEL.2015.2426200

position estimation algorithm developed relies on how accurately $\Delta i/\Delta t$ may be estimated, which is sensitive to current measurement noise, and it is often difficult to use, e.g., current oversampling to help to improve the signal-to-noise ratio. Without using any injection voltage also means that the resultant current variation to be measured is not under control, which may be too small to be measured accurately due to low back-EMF voltage [14], [15].

An example method based on current variation measurement is the well-known INFORM method [16], [17], with controllable injection voltage vectors to secure reliable Δi to be measured. A simple form to use the INFORM method is to inject three separate voltage vectors along phase axes for position estimation [17]. Other methods using at least two separate injection voltage vectors are reported in [11], [18], and [24], utilizing the current variation behavior under different injected voltage vectors. The resultant estimator is believed to be more sensitive to current measurement errors since subtraction or division of separately measured current variation magnitudes is used for rotor position calculations. All these methods rely on accurate measurement of the current variation magnitude caused by the injected voltage. Considering measurement noise, it will be an advantage to use the sign of the current variation only to predict, e.g., the polarity of the position error directly. Besides this, the inverter voltage error effects on the above proposed methods have not been well discussed, which is worth to consider in practical applications.

In this paper, a new algorithm using ideally a single voltage injection vector is introduced. The resultant current variation under this single testing voltage vector is directly linked to the position error. No filters are needed for extracting the high-frequency current signals and use of low-pass filters (LPFs) in the current control loop of the FOC is not needed. The proposed method is also further developed to reduce the effects of the inverter voltage error on the position estimation accuracy by injecting two opposite voltage vectors. In Section II, control fundamentals for the PMSM are given. The new approach is explained in detail in Section III. Various experimental results are given in Section IV. Section V concludes this paper.

II. Control Fundamentals for PMSM

A. Modeling of PMSM

The voltage equations of the PMSM represented in the rotor *dq*-reference frame are well known, as

$$\begin{cases} v_d = Ri_d + L_d \dfrac{d}{dt} i_d - \omega_r L_q i_q \\ v_q = Ri_q + L_q \dfrac{d}{dt} i_q + \omega_r L_d i_d + \omega_r \lambda_{mpm} \end{cases} \tag{1}$$

where v_d, v_q, i_d, i_q are the stator d-axis and q-axis voltages and currents, respectively; L_d and L_q are the d-axis and q-axis inductances; R is the stator resistance; ω_r is the rotor speed; and λ_{mpm} is the peak value of the rotor PM flux linkage. This equation is represented in the machine real *dq*-reference frame; therefore, it cannot be used directly for position estimation. It is often needed to transfer (1) to either the estimated *dq*-reference frame or the stationary $\alpha\beta$-reference frame for rotor position estimation. In the $\alpha\beta$-reference frame, when using the vector representation, (1) may be conveniently expressed in a compact form as

$$\begin{aligned} \bar{v}_{\alpha\beta} = {} & R\bar{i}_{\alpha\beta} + \left(L_1 \frac{d}{dt} \bar{i}_{\alpha\beta} + L_2 \frac{d}{dt} \bar{i}^*_{\alpha\beta} e^{j2\theta_r} \right) \\ & + j2\omega_r L_2 \bar{i}^*_{\alpha\beta} e^{j2\theta_r} + j\omega_r \lambda_{mpm} e^{j\theta_r} \end{aligned} \tag{2}$$

where $L_1 = (L_d + L_q)/2$, $L_2 = (L_d - L_q)/2$, $\bar{i}^*_{\alpha\beta}$ is the conjugate vector of $\bar{i}_{\alpha\beta}$, and θ_r is the rotor position. The term with the position associated to the rotor PM flux linkage λ_{mpm} is used in the back-EMF-based sensorless controllers. The position may also be estimated from the terms associated to the inductance L_2. It is clear that L_d and L_q must not be equal if the position information needs to be extracted from those terms involving inductance L_2, and it is always twice the rotor position ($2\theta_r$) that may be estimated directly.

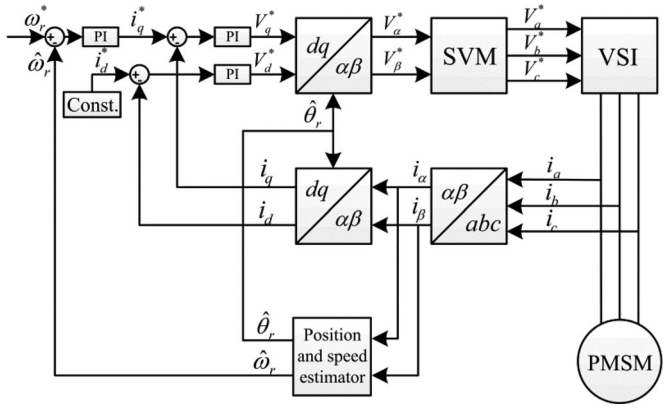

Fig. 1. Typical sensorless FOC system for PMSM.

B. FOC System for PMSM

The FOC method of PMSM has been widely used for PMSM drive system. Its classical controller topology is shown in Fig. 1. The controller is realized in the real machine *dq*-reference frame. The rotor speed is used as the feedback signal, which compares with the reference speed, and the error drives a PI controller to determine the q-axis current (torque) reference. The voltage commands in the *dq*-reference frame are given by the two current control-loop PI controllers. To transfer the measured currents to the *dq*-current components and to convert *dq*-voltage commands to the $\alpha\beta$ voltage commands, the rotor position information is needed. In sensorless control, the rotor position as well as the rotor speed information needs to be provided from particular estimators. Such estimators may use the machine terminal voltage, line current, and machine parameters to estimate the rotor position. As the simplest case, the position may be estimated using the measured current only, as indicated in Fig. 1. The speed may often be estimated by using a PLL, as it will be shown later.

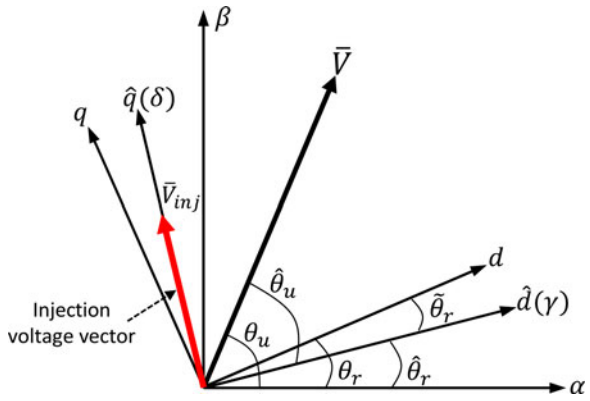

Fig. 2. Real and estimated rotor reference frames.

III. Proposed Sensorless Algorithm

A. Principle of the Proposed Method

When the PMSM operates at a very low speed, the rotor speed $\omega_r \approx 0$ and the last two terms in (2) associated with ω_r may then be eliminated. By neglecting the stator resistance, which may be achieved when selecting an injection voltage $\bar{v}_{\alpha\beta} \gg R\bar{i}_{\alpha\beta}$, (2) may then be approximated by more voltage than the one that the resistance is taking is injected

$$\bar{v}_{\alpha\beta} = L_1 \frac{d}{dt}\bar{i}_{\alpha\beta} + L_2 \frac{d}{dt}\bar{i}^*_{\alpha\beta} e^{j2\theta_r}. \tag{3}$$

Solving (3) for $d\bar{i}_{\alpha\beta}/dt$, it may be obtained that

$$\frac{d}{dt}\bar{i}_{\alpha\beta} = \frac{1}{L_1^2 - L_2^2}\left(L_1 \bar{v}_{\alpha\beta} - L_2 \bar{v}^*_{\alpha\beta} e^{j2\theta_r}\right). \tag{4}$$

In one switching period, the current differentiation $d\bar{i}_{\alpha\beta}/dt$ may be approximated by $\Delta\bar{i}_{\alpha\beta}/\Delta t$. Therefore, the current variation may be expressed as

$$\Delta\bar{i}_{\alpha\beta} = \left(c_1 + c_2 e^{j2(\theta_r - \theta_u)}\right)\Delta t \cdot \overline{V}_{\alpha\beta} \tag{5}$$

where $c_1 = L_1/(L_1^2 - L_2^2)$, $c_2 = -L_2/(L_1^2 - L_2^2)$. θ_u is the voltage vector angle in the $\alpha\beta$-reference frame, i.e., $\overline{V}_{\alpha\beta} = V_m e^{j\theta_u}$. This is the fundamental equation for deriving, e.g., the INFORM method [16], [17].

In the INFORM method, three voltage vectors may be injected along the phase-*a*, phase-*b*, and phase-*c* axes, respectively [16], [17]. The corresponding phase current variations are measured and used in (5) for extracting the rotor position. Actually, it will be more convenient to transform (5) to the estimated rotor reference frame, where it allows to use only one injected voltage vector for position estimation.

For transforming (5) from the $\alpha\beta$-reference frame to the estimated *dq*-reference frame (also noted as the $\gamma\delta$-reference frame), the estimated rotor position $\hat{\theta}_r$ is introduced, as shown in Fig. 2. By multiplying $e^{-j\hat{\theta}_r}$ on both sides of (5), it may be derived that

$$\Delta\bar{i}_{\gamma\delta} = \Delta\bar{i}_{\alpha\beta} e^{-j\hat{\theta}_r} = \left(c_1 + c_2 e^{j2\left(\theta_r - \hat{\theta}_r - \hat{\theta}_u\right)}\right)\Delta t \bar{V}_{\gamma\delta} \tag{6}$$

where $\bar{V}_{\gamma\delta}$ is the voltage vector represented with respect to the estimated *d*-axis (γ-axis), with the local angle of $\hat{\theta}_u = \theta_u - \hat{\theta}_r$.

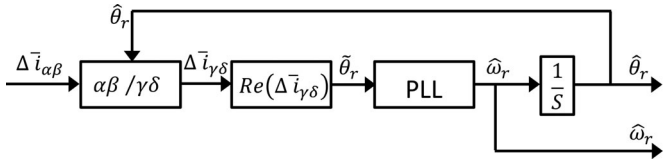

Fig. 3. Block diagram of the PLL controller for recovering the rotor position and speed from the estimated position error.

Therefore, for example, if choosing the injected voltage vector to be aligned with the estimated *q*-axis (δ-axis), then $\hat{\theta}_u = \pi/2$, $\bar{V}_{\gamma\delta} = V_m e^{j\pi/2}$, as indicated in Fig. 2. With this injection voltage, (6) may then be rewritten as

$$\begin{aligned}\Delta\bar{i}_{\gamma\delta} = {} & \Delta t c_2 V_m \sin\left(2\tilde{\theta}_r\right) \\ & + j\left(\Delta t c_1 V_m - \Delta t c_2 V_m \cos\left(2\tilde{\theta}_r\right)\right)\end{aligned} \tag{7}$$

where $\tilde{\theta}_r = \theta_r - \hat{\theta}_r$ is the rotor position error. Such injection voltage vector will isolate the sine component of the position error to the real part of (7) only. Therefore, the measured current variation on the estimated *d*-axis (γ-axis) will be directly linked to the position error, as

$$\mathrm{Re}\left(\Delta\bar{i}_{\gamma\delta}\right) = \Delta\bar{i}_{\gamma} = k \cdot \sin\left(2\tilde{\theta}_r\right) \propto 2k \cdot \tilde{\theta}_r \tag{8}$$

where $k = \Delta t c_2 V_m$, which is a constant. The estimated rotor position angle $\hat{\theta}_r$ and the estimated rotor speed $\hat{\omega}_r$ may then be obtained by using the classical PLL controller [23], as shown in Fig. 3. The design of the PLL parameters have been well explained by using analytical approximations based on the accurate time domain response of the PLL to a unit-step input [23].

It is worth to notice that it is also possible to inject the voltage vector on the estimated *d*-axis (γ-axis). With $\hat{\theta}_u = 0$ and $\bar{V}_{\gamma\delta} = V_m e^{j0}$, (6) may be developed to

$$\begin{aligned}\Delta\bar{i}_{\gamma\delta} = {} & \Delta t c_1 V_m + \Delta t c_2 V_m \cos\left(2\tilde{\theta}_r\right) \\ & + j\Delta t c_2 V_m \sin\left(2\tilde{\theta}_r\right).\end{aligned} \tag{9}$$

Then the imaginary part of the current variation vector in the $\gamma\delta$-reference frame may be linked to the position error as

$$\mathrm{Im}\left(\Delta\bar{i}_{\gamma\delta}\right) = \Delta\bar{i}_{\delta} = k \cdot \sin\left(2\tilde{\theta}_r\right) \propto 2k \cdot \tilde{\theta}_r. \tag{10}$$

B. Implementation of the Proposed Method

In the implementation, the needed voltage vector will be injected once every two switching periods. Fig. 4 shows the voltage injection scheme in connection to the FOC control period where the voltage determined by the PI controllers will be updated. Similar to many other injection methods, by separating the FOC control period and the injection period, the current variation due to the injected voltage may be reliably measured. The switching frequency is set to be 10 kHz as an example, and the injection frequency will be half of the switching frequency.

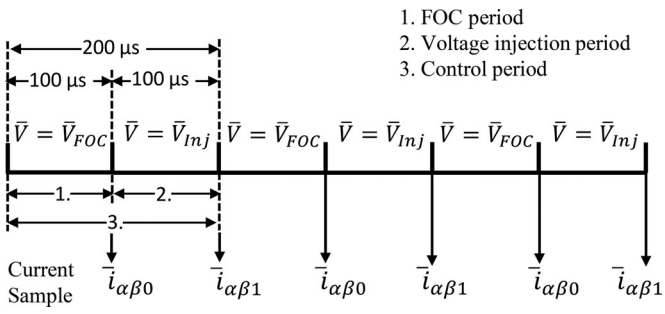

Fig. 4. Implementation of voltage injection scheme for PMSM.

The current at the beginning of each switching period is measured. The measured current variation during the voltage injection period is used for position estimation, as (8), or (10). The PI controller will respond to the current sampled in the beginning of FOC control period only. Therefore, by separating the FOC control period and the voltage injection period, no filter is needed to extract the high-frequency current ripples for position estimation or to obtain the fundamental current component.

Considering that the rotor position angle may be assumed to be constant during one switching period, the current variation $\Delta\bar{i}_{\alpha\beta}$ measured in the $\alpha\beta$-reference frame may be transferred to the $\gamma\delta$-reference frame by multiplying $e^{-j\hat{\theta}_r}$. Therefore, the desired current change in the $\gamma\delta$-reference frame may be obtained by

$$\Delta\bar{i}_{\gamma\delta} = (\Delta i_\alpha + j\Delta i_\beta)\left(\cos\hat{\theta}_r - j\sin\hat{\theta}_r\right) \tag{11}$$

and consequently referring to Fig. 4, the current variation that is directly linked to the position error may be obtained as

$$\mathrm{Re}\left(\Delta\bar{i}_{\gamma\delta}\right) = (i_{\alpha 1} - i_{\alpha 0})\cos\hat{\theta}_r + (i_{\beta 1} - i_{\beta 0})\sin\hat{\theta}_r \tag{12}$$

$$\mathrm{Im}\left(\Delta\bar{i}_{\gamma\delta}\right) = -(i_{\alpha 1} - i_{\alpha 0})\sin\hat{\theta}_r + (i_{\beta 1} - i_{\beta 0})\cos\hat{\theta}_r. \tag{13}$$

Now, one injected voltage vector will be enough for the rotor position estimation. This could also be a simple voltage injection scheme for sensorless control of PMSM.

C. Minimization of Inverter Voltage Error Effects

In low-speed operation, the performance of the sensorless drive is often influenced by the voltage error caused by inverter nonlinearities [13]. Due to the existence of the inverter voltage error, the injected voltage vector may not be located on the desired axis, resulting in an estimation error.

As it may be observed from (5), the coefficient c_1 is much greater than c_2. In the proposed method, when the voltage is injected on the δ-axis, the term associated to c_1 will only appear in the imaginary part of (7). The position error is estimated by utilizing the real part of (7) and eliminating the effects caused by the large coefficient c_1. The INFORM method uses very similar principle. For example, by injecting three voltage vectors along phase-*a*, phase-*b*, and phase-*c* axes, respectively, the terms associated to coefficient c_1 can finally be eliminated [16], [17]. The term associated to c_2 is then used for position estimation. If the voltage vector cannot be injected on the desired axis due to the inverter voltage error, then the term associated to c_1 cannot be totally eliminated in the position estimation. A small voltage error may be enlarged by the large coefficient c_1, affecting the position estimation accuracy. This is why it has been suggested to use additional voltage sensors to achieve satisfactory results when using the INFORM method [12], which is not a convenient solution.

The inverter voltage error may be compensated before being applied to the motor terminals. But the voltage error caused by inverter nonlinearity depends both on the magnitude and direction of the machine current vector [19]–[21]. The error in, e.g., determining the instantaneous location of the current vector may affect the voltage error compensation accuracy. In addition, the voltage error caused by inverter dead-time depends on the current magnitude as well, due to very small snubber and parasitic capacitance [22]. An accurate voltage error compensation needs to know these capacitance values, which is not easy especially when including the parasitic capacitance of, e.g., a long cable between the inverter and the motor.

The proposed injection method for position estimation may be improved to reduce the inverter voltage error by adding one more injection voltage. For example, in the first injection period, the voltage vector is injected on the δ-axis ($V_m e^{j\pi/2}$). Then, a second voltage on the minus δ-axis is injected ($V_m e^{-j\pi/2}$) consequently in the following switching period. Assuming the inverter voltage error, denoted as $\Delta\bar{V}$, will not change during these two switching periods, the actual voltage vectors supplied to the machine terminals may be expressed as

$$\overline{V}_{\gamma\delta 1} = V_m e^{j\hat{\theta}_{u1}} \approx V_m e^{j\pi/2} - \Delta\overline{V} \tag{14}$$

$$\overline{V}_{\gamma\delta 2} = V_m e^{j\hat{\theta}_{u2}} \approx V_m e^{-j\pi/2} - \Delta\overline{V} \tag{15}$$

where subscripts 1 and 2 denote the first injection period and the second injection period, respectively.

Therefore, by following (6), the resultant current variations viewed in the local $\gamma\delta$-reference may be found to be

$$\Delta\bar{i}_{\gamma\delta 1} = \Delta tc_1\left(V_m e^{j\pi/2} - \Delta\overline{V}\right) + \Delta tc_2 e^{j2\tilde{\theta}_r}\cdot e^{-j\hat{\theta}_{u1}} V_m \tag{16}$$

$$\Delta\bar{i}_{\gamma\delta 2} = \Delta tc_1\left(V_m e^{-j\pi/2} - \Delta\overline{V}\right) + \Delta tc_2 e^{j2\tilde{\theta}_r}\cdot e^{-j\hat{\theta}_{u2}} V_m. \tag{17}$$

Referring to Fig. 5, it may be observed that $\hat{\theta}_{u1} = \pi/2 + \Delta\theta_{u1}$, $\hat{\theta}_{u2} = -\pi/2 - \Delta\theta_{u2}$, and $\Delta\theta_{u1} \approx \Delta\theta_{u2}$. It is not difficult to derive that

$$\mathrm{Re}\left(\Delta\bar{i}_{\gamma\delta 1} - \Delta\bar{i}_{\gamma\delta 2}\right) = 2\Delta tc_2 V_m \cos\left(\Delta\theta_{u1}\right)\sin 2\left(\tilde{\theta}_r\right). \tag{18}$$

Since the angle $\Delta\theta_{u1}$ is very close to zero. Therefore

$$\mathrm{Re}\left(\Delta\bar{i}_{\gamma\delta 1} - \Delta\bar{i}_{\gamma\delta 2}\right) = 2k\sin\left(2\tilde{\theta}_r\right) \approx 4k\tilde{\theta}_r \tag{19}$$

where k is the gain used in (8). Equation (19) shows very similar result to the case studied, when the inverter voltage error is neglected, e.g., in (8).

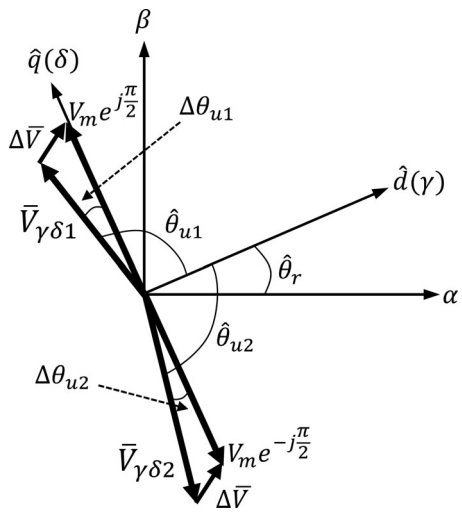

Fig. 5. Opposite voltage injection scheme that may help to reduce voltage error effects.

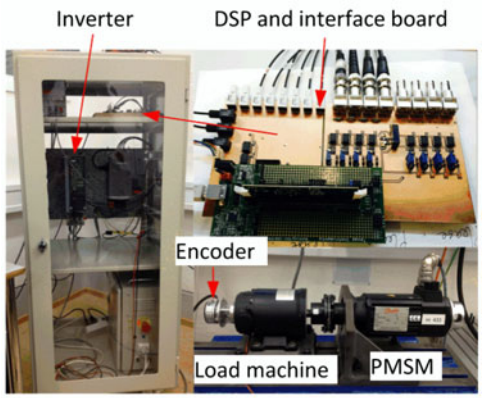

Fig. 6. Experimental platform for testing the new sensorless control method.

Similar opposite voltage vectors may be injected on the γ-axis, i.e., along the positive γ-axis ($V_m e^{j0}$) and along the negative γ-axis ($V_m e^{j\pi}$). By following the same steps described earlier, the position error may be linked to the imaginary part of the current variations terms as

$$\mathrm{Im}\left(\Delta\bar{i}_{\gamma\delta 1} - \Delta\bar{i}_{\gamma\delta 2}\right) = 2k\sin\left(2\tilde{\theta}_r\right) \approx 4k\tilde{\theta}_r. \qquad (20)$$

It is worth to mention that since the injected voltage vectors are opposite to each other, therefore, $\Delta\bar{i}_{\gamma\delta 1}$ and $\Delta\bar{i}_{\gamma\delta 2}$ have opposite signs.

IV. Experimental Results

The proposed method discussed in Section III is tested on an experimental drive system. As shown in Fig. 6, the experimental platform employs a PMSM, a dc motor as the load, a Digital Signal Processor (DSP-F28335) controller, and a Danfoss FC302 inverter designed for automation drives. An incremental encoder with 2048 lines per revolution is used for obtaining the real rotor position for comparison. The parameters of the PMSM machine are listed in Table I. In the experiment, the switching frequency

TABLE I
PMSM Specifications

Parameters of SMPMSM			
Rated power (W)	470	Stator resistance (Ω)	2.35
Max. phase voltage (V)	380	*d*-axis inductance (mH)	10
Rated current (A)	2.9	*q*-axis inductance (mH)	13.4
Rated speed (r/min)	2850	PM flux linkage (Wb)	0.133
Rated frequency (Hz)	95	Pole pairs	2

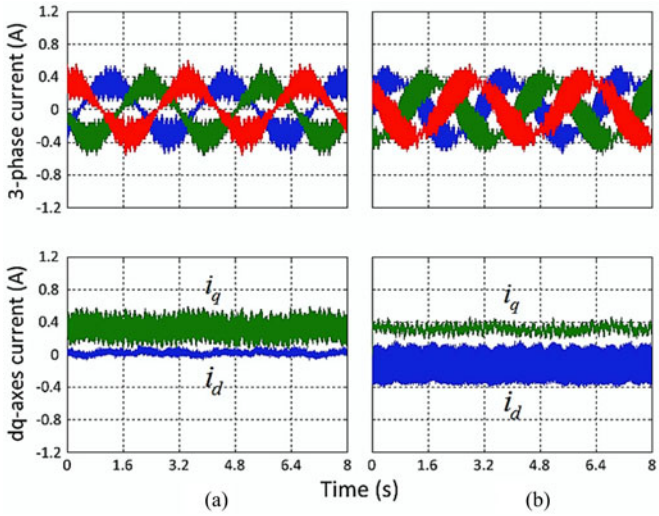

Fig. 7. Steady-state current in the machine real *dq*-reference frame for the two proposed injection methods. (a) Voltage injected on the δ-axis. (b) Voltage injected on the γ-axis.

of the inverter was chosen to be 10 kHz as an example. The current is sampled at the beginning of each switching period. Hardware antialiasing *RC* filters ($R = 683\ \Omega$, $C = 1$ nF) are used to improve the signal-to-noise ratio of the current measurement. Selection of the injection voltage vector magnitude is an important issue for almost all kinds of high-frequency injection methods in implementation and for different sizes of electrical machines. It is clear that the resultant current variation increases when the magnitude of the injected voltage vector is increased. This improves the signal-to-noise ratio and will give better estimation performance, as experimentally illustrated in [24]. But at the same time, the increased current ripple will cause more torque ripple and reduce the drive performance. In the low-speed operation range, selection of the magnitude of the injection voltage vector is not mainly restricted by the maximum available inverter output voltage but is rather a compromise between the position estimation performance and the drive performance. This is a common problem for various high-frequency injection methods. In this application, a desired current variation within one switching period was chosen to be roughly around 0.15 A and the corresponding required voltage vector magnitude was found to be 45 V.

The drive with the proposed sensorless control method is tested under various conditions. The proposed method is developed based on the same fundamental machine equation (3) as the

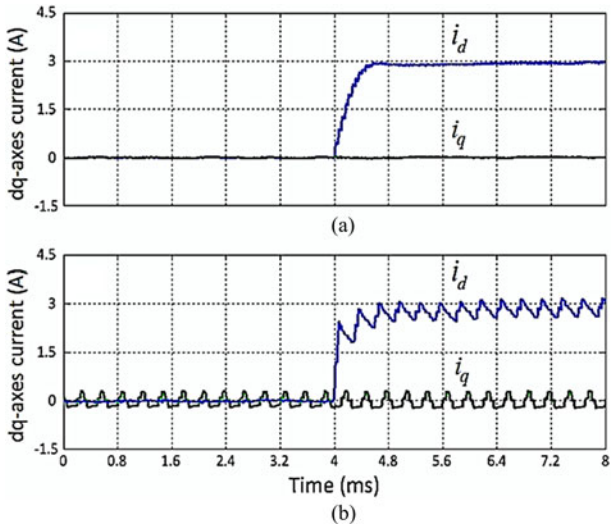

Fig. 8. Current response with/without voltage injection for position estimation. (a) Without voltage injection. (b) With voltage injection on the δ-axis.

INFORM method. Therefore, comparison to the INFORM method is given in this section. The influence of the injection voltage on the current and the effectiveness of suppressing the influence of inverter voltage error on the position estimation accuracy are demonstrated.

A. Influence of Injection Voltage on the Current

In this experiment, the real rotor position and speed are used and the motor is controlled in steady state with no load. The voltage is injected on the γ-axis and δ-axis, respectively, and the position is estimated by using (10) and (8), correspondingly. The resultant current ripples are shown in Fig. 7.

It may be observed from Fig. 7(a) that when the voltage is injected on the δ-axis, the real q-axis current will have a larger ripple, as expected. The peak-to-peak value of the q-axis current ripple is around 0.5 A, and the ripple of the d-axis current is much smaller. Fig. 7 (b) shows that when the voltage is injected on the γ-axis, the peak-to-peak q-axis current ripple can be greatly reduced to around 0.15 A. According to the torque equation of a PMSM, the q-axis current has a predominant influence on the torque. Therefore, it is preferred to inject the voltage on the γ-axis [see Fig. 7 (b)], which can reduce the q-axis current ripple and consequently the torque ripple.

It is worth mentioning that in the proposed injection method, no filter is needed in the current control loop in order to extract the position information from the resultant current ripples. Therefore, the proposed injection method will have little influence on the control bandwidth of the current control loop.

Fig. 8 shows the current step responses with and without the injection method at standstill. The d-axis current step command is given so the machine will not rotate during this transient period. For comparing the performances of the current-loop controllers, the same parameters are used in the PI controllers with/without the voltage injection. Fig. 8(a) shows the d-axis current response without the injection voltage and Fig. 8 (b) shows the d-axis current response with a voltage injected on the δ-axis. It may be observed that the rise time of the d-axis current is very similar when comparing Fig. 8(a) with (b). This is mainly due to that the pole corresponding to the delay caused by the additional injection period is far away from the imaginary axis in the s-place and its influence is not dominant. The current variation on the d-axis after 4 ms in Fig. 8(b) is due to that the d-axis voltage is applied every two switching periods (see Fig. 4). During the switching period when the testing voltage is injected on the q-axis only, the d-axis current will decrease naturally.

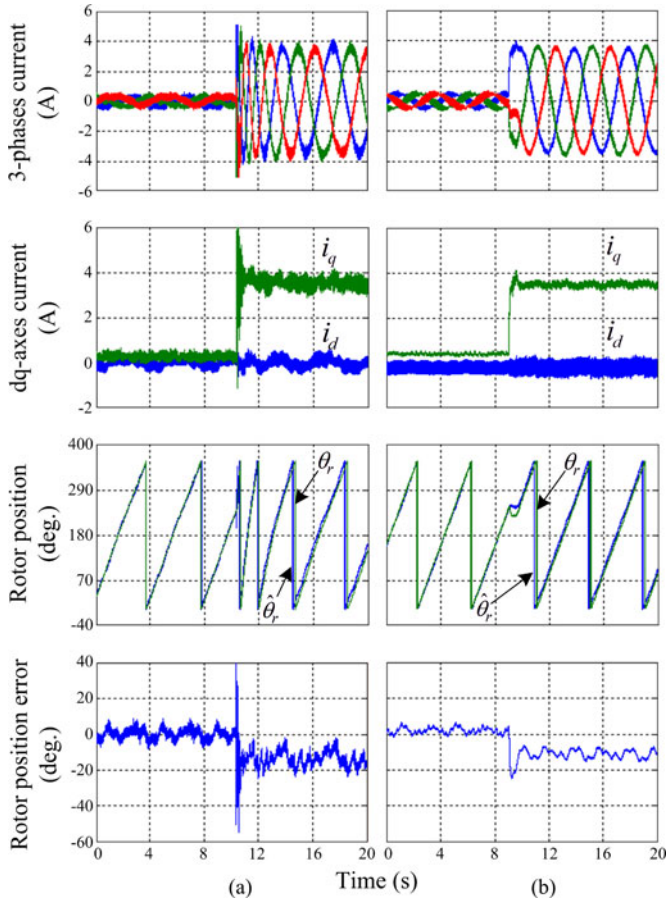

Fig. 9. Comparison of the INFORM method [16], [17] versus the γ-axis injection method at 7.5 r/min operation condition. From top to bottom: three-phase currents; current in the real dq-reference frame; real and estimated rotor position; the position error. (a) INFORM method; (b) γ-axis injection method.

B. Comparison with the INFORM Method

For comparing with the traditional INFORM method, the γ-axis injection method and the INFORM method with three injection voltage vectors along phase axes [16], [17] are both implemented in the test drive system. The switching frequency is 10 kHz. Therefore, the updating frequency of the controller for the INFORM method is 2.5 kHz, and for the γ-axis injection method, it is 5 kHz. The magnitudes of the injection voltage are the same. The rotor position and speed used in FOC are both obtained from the encoder so the estimated position error

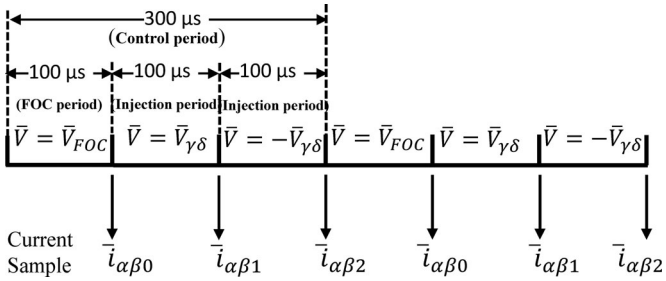

Fig. 10. Modified voltage injection sequence.

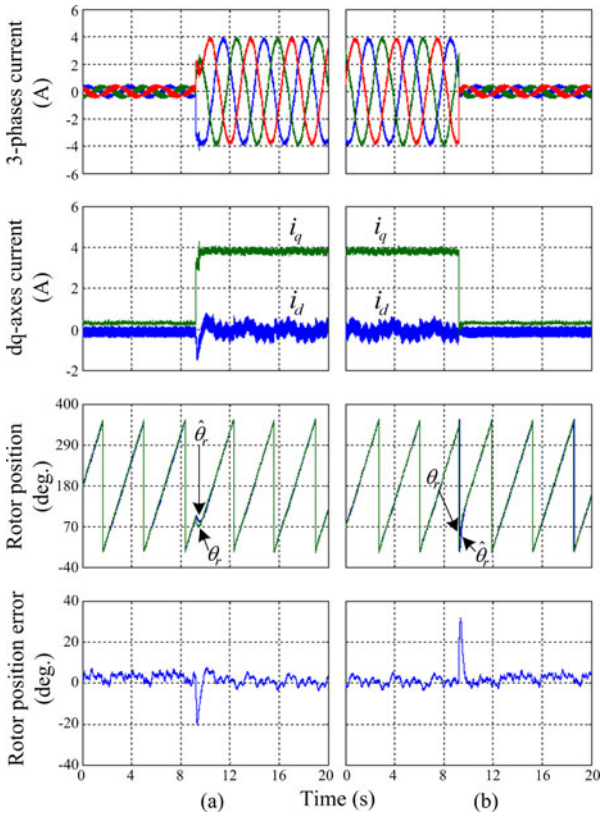

Fig. 11. Torque step with $\hat{\theta}_r$ at 9 r/min, with opposite voltage injected on the γ-axis. From top to bottom: three-phase currents; current in the real dq-reference frame; real and estimated rotor position; the position error.

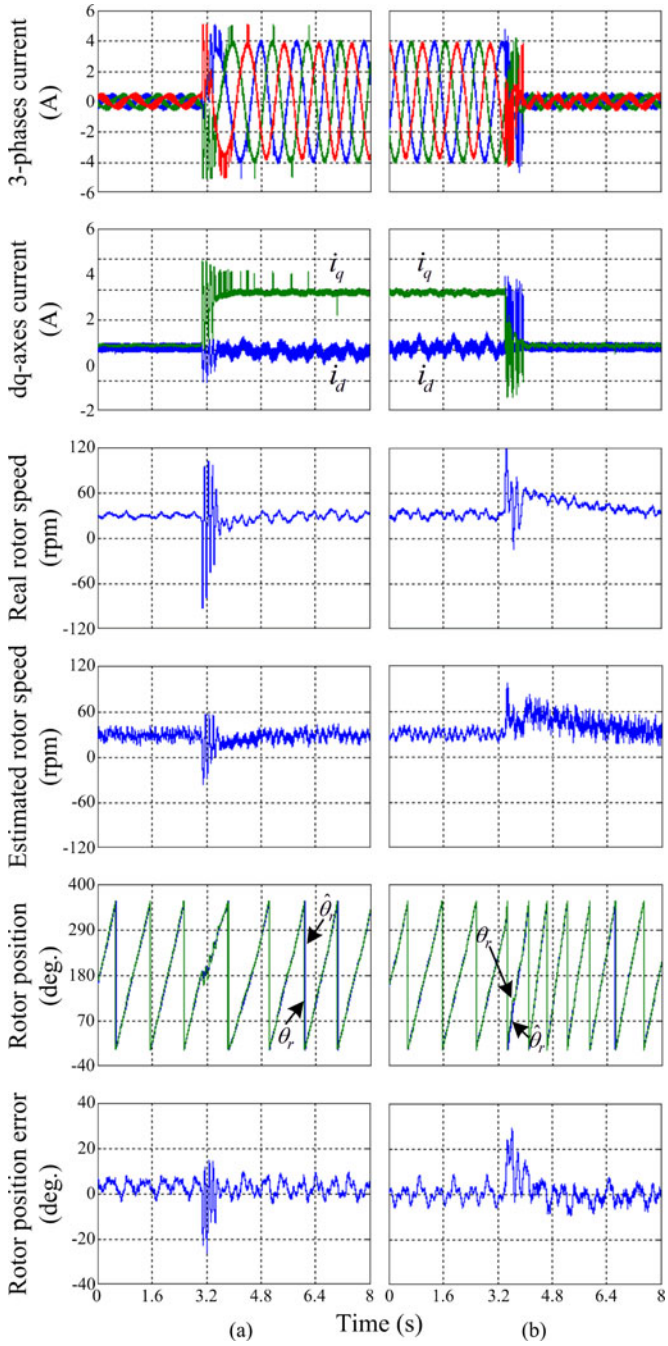

Fig. 12. Torque step response using estimated position $\hat{\theta}_r$ and speed $\hat{\omega}_r$ at 30 r/min operation condition. From top to bottom: three-phase currents; current in the real dq-reference frame; real rotor speed; estimated rotor speed; real and estimated rotor position; and the position error.

from these two methods will not affect the drive performance. As shown in Fig. 9(a), when the INFORM method is used in the system, the q-axis current has a larger current ripple of around 0.5 A with respect to its dc component. The INFORM method generates $\pm 8°$ ripple in the estimated rotor position error at no load. For the γ-axis injection method, the ripple in the estimated rotor position is around $\pm 3.5°$ with respect to its dc value. When a load torque is applied to the machine, both methods give a visible dc offset in the estimated rotor position (around $-12°$). The ripple in the estimated rotor position for the INFORM method increases to $\pm 10.5°$, and this ripple becomes $\pm 5°$ for the proposed γ-axis injection method. This dc bias is very likely caused by the inverter voltage error [21], [22]. It is interesting to notice that similar dc bias position error may also be observed in other methods [7]–[11], [14], [25], where this dc bias error could be up to 18°–28° when running at low speed [25].

It may also be noticed that as shown in Fig. 9, after the load is applied, the INFORM method gives larger transient position error as compared to the proposed γ-axis injection method. This may be due to the fact that the INFORM method uses three injection voltage vectors, and there is only one injection voltage vector in the proposed γ-axis injection method. The existence

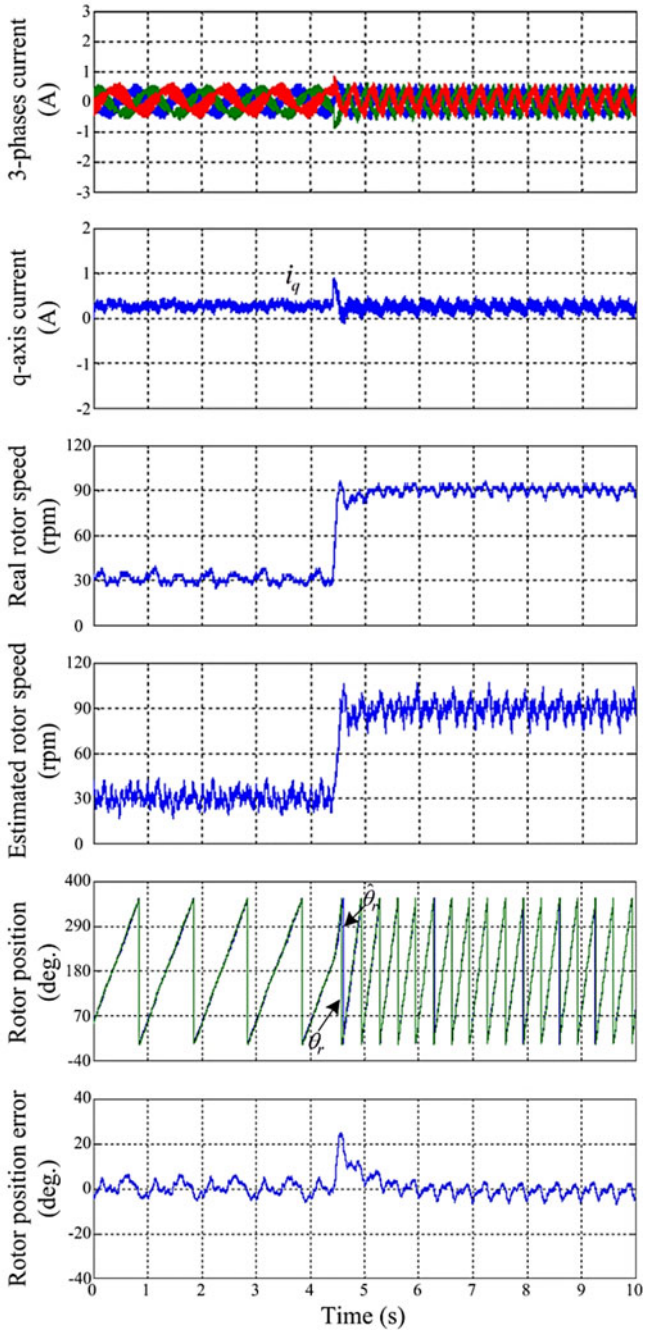

Fig. 13. Speed step change response from 30 to 90 r/min using estimated position $\hat{\theta}_r$ and speed $\hat{\omega}_r$. From top to bottom: three-phase currents; machine real q-axis current; real rotor speed; estimated rotor speed; real and estimated rotor position; and the position error.

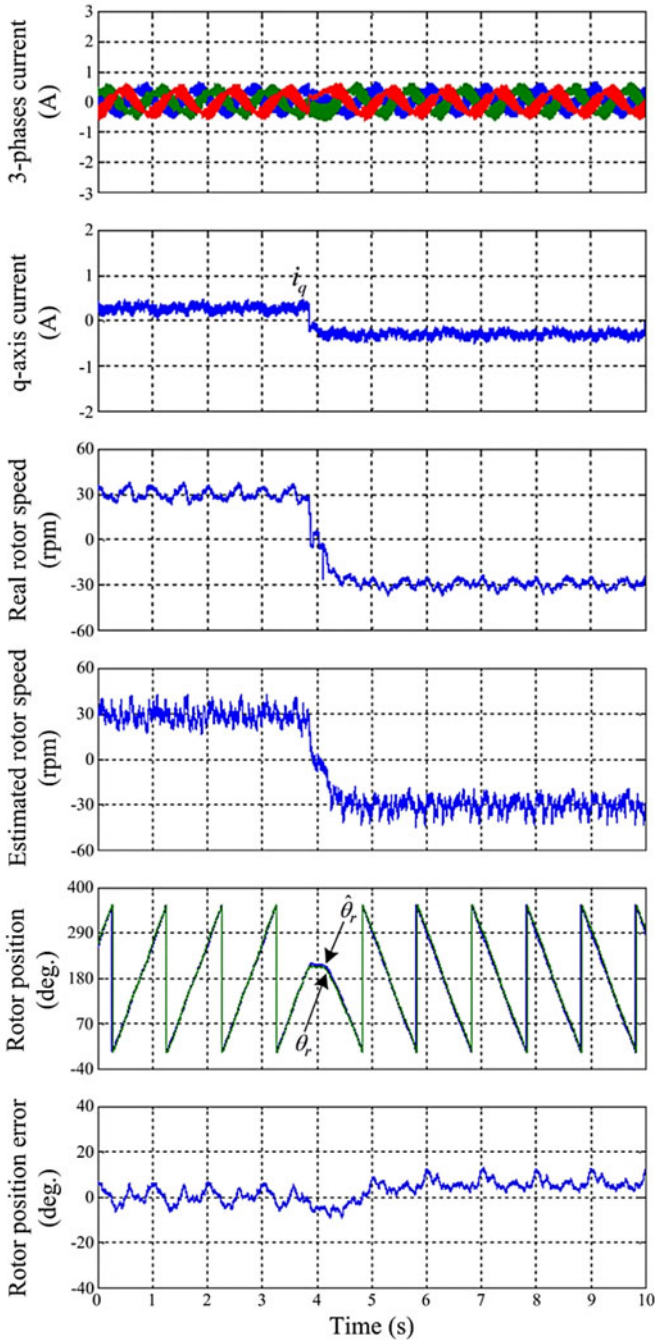

Fig. 14. Speed reversal response from 30 to -30 r/min using estimated position $\hat{\theta}_r$ and speed $\hat{\omega}_r$. From top to bottom: three-phase currents; machine real q-axis current; real rotor speed; estimated rotor speed; real and estimated rotor position; and the position error.

of inverter voltage error will bring position estimation error to both methods. When more injection voltage vectors are used, the more sensitive the method might be on, e.g., the inverter voltage error. This comparison has also shown that the proposed method is more robust than the INFORM method.

C. With Inverter Voltage Error Effects Reduction

In Section III-C, it was proposed that by adding one more injection voltage, the influence of the inverter voltage error may be reduced. The new injection scheme is illustrated in Fig. 10, in which, following the FOC control period (PI control period) for updating the output voltage, two voltage vectors with opposite directions are injected consequently.

Fig. 11 shows the measured results of the improved method with one more injection voltage as described in Section III-C and Fig. 10. The two opposite voltage vectors are injected on the γ-axis. In this experiment, the estimated rotor position is used as the feedback for the current control loop. The speed is from the

encoder. Load torque step is introduced for examining the transient performance. Compared to the results shown in Fig. 9 (b), where only one injection voltage is used, the dc offset in the estimated position has now been largely compensated. The ripple in the estimated position when working in steady state is around $\pm 3°$.

D. Full Sensorless Control

In this experiment, the estimated speed from the PLL is used as the feedback for the speed loop. The drive is then under full sensorless control. The drive performance experiencing a step load torque change is shown in Fig. 12.

As it may be observed from Fig. 12, the drive can well survive the nearly full-load torque change working conditions. It is worth mentioning that when the q-axis current is maintained at 4 A, the peak-to-peak q-axis current ripple is 0.15 A (around 4% of the desired dc component of the q-axis current) only.

Figs. 13 and 14 show the full sensorless drive system performances when the reference speed command has a step change (see Fig. 13), and the speed command is reversed (see Fig. 14). The drive shows good performance in general in these different working conditions. In the speed reversal experiment, during the transient, the position error is well maintained below 10 elect. degrees, as it may be observed from Fig. 14.

V. Conclusion

In this paper, a voltage injection scheme using ideally one injection voltage vector is presented. The influence of the inverter voltage error on the estimated position error is analyzed and solution to overcome this difficulty is proposed. No filter is required for position estimation in the current control loop and the proposed injection method has a little effect on the current control loop bandwidth, resulting in fast current regulation as normal FOC. It is simple to implement the proposed algorithm, resulting in lower computation burden and better accuracy compared to available methods such as the INFORM method. The experimental results have shown that such sensorless drive exhibits good performance in both steady state and different transient operation conditions.

References

[1] J. Holtz, "Developments in sensorless ac drive technology," in *Proc. Int. Conf. Power Electron. Drives Syst.*, Nov./Dec. 2005, vol. 1, pp. 9–16.

[2] R. S. Wu and G. R. Slemon, "A permanent magnet motor drive without a shaft sensor," *IEEE Trans. Ind. Appl.*, vol. 27, no. 5, pp. 1005–1011, Sep./Oct. 1991.

[3] I. Boldea, M. C. Paicu, and G. D. Andreescu, "Active flux concept for motion-sensorless unified AC drives," *IEEE Trans. Power Electron.*, vol. 23, no. 5, pp. 2612–2618, Sep. 2008.

[4] F. Genduso, R. Miceli, C. Rando, and G. R. Galluzzo, "Back EMF sensorless-control algorithm for high-dynamic performance PMSM," *IEEE Trans. Ind. Electron.*, vol. 57, no. 6, pp. 2092–2100, Jun. 2010.

[5] K. Lu, L. Xiao, and F. Blaabjerg, "Artificial inductance concept to compensate nonlinear inductance effects in the back EMF-based sensorless control method for PMSM," *IEEE Trans. Energy Convers.*, vol. 28, no. 3, pp. 593–600, Sep. 2013.

[6] B. N. Mobarakeh, F. M. Tabar, and F-M. Sargos, "Back-EMF estimation based sensorless control of PMSM: Robustness with respect to measurement errors and inverter irregularities," in *Proc. Conf. Rec. 2004 IEEE 39th IAS Annu. Meeting*, Oct. 2004, vol. 3, pp. 1858–1865.

[7] M. J. Corley and R. D. Lorenz, "Rotor position and velocity estimation for a salient-pole permanent magnet synchronous machine at standstill and high speeds," *IEEE Trans. Ind. Appl.*, vol. 34, no. 4, pp. 784–789, Jul./Aug. 1998.

[8] J. H. Jang, S. K. Sul, J. I. Ha, K. Ide, and M. Sawamura, "Sensorless drive of surface-mounted permanent-magnet motor by high-frequency signal injection based on magnetic saliency," *IEEE Trans. Ind. Appl.*, vol. 39, no. 4, pp. 1031–1039, Jul./Aug. 2003.

[9] J. Holtz, "Acquisition of position error and magnet polarity for sensorless control of PM synchronous machines," *IEEE Trans. Ind. Appl.*, vol. 44, no. 4, pp. 1172–1180, Jul./Aug. 2008.

[10] J. M. Liu and Z. Q. Zhu, "Novel sensorless control strategy with injection of high-frequency pulsating carrier signal into stationary reference frame," *IEEE Trans. Ind. Appl.*, vol. 50, no. 4, pp. 2574–2583, Jul./Aug. 2014.

[11] D. Paulus, P. Landsmann, and R. Kennel, "Sensorless field-oriented control for permanent magnet synchronous machines with an arbitrary injection scheme and direct angle calculation," in *Proc. Symp. Sensorless Control Elect. Drives*, Sep. 2011, pp. 41–46.

[12] Y. D. Yoon, S. K. Sul, and K. Ide, "High-bandwidth sensorless algorithm for AC machine based on square-wave-type voltage injection," *IEEE Trans. Ind. Appl.*, vol. 47, no. 3, pp. 1361–1370, May/Jun. 2011.

[13] D. Raca, P. Garcia, D. D. Reigosa, F. Briz, and R. D. Lorenz, "Carrier-signal selection for sensorless control of PM synchronous machines at zero and very low speeds," *IEEE Trans. Ind. Appl.*, vol. 46, no. 1, pp. 167–178, Jan./Feb. 2010.

[14] C. Y. Wang and L. Y. Xu, "A novel approach for sensorless control of PM machines down to zero speed without signal injection or special PWM technique," *IEEE Trans. Power Electron.*, vol. 19, no. 6, pp. 1601–1607, Nov. 2004.

[15] R. Raute, C. Caruana, C. S. Staines, J. Cilia, M. Sumner, and G. Asher, "Operation of a sensorless PMSM drive without additional test signal injection," in *Proc. 4th IET Conf. Power Electron., Machines Drives*, Apr. 2008, pp. 616–620.

[16] M. Schroedl, "Sensorless control of AC machines at low speed and standstill based on the 'INFORM' method," in *Proc. Conf. Record 1996 IEEE 31st IAS Annual Meeting*, Oct. 1996, vol. 1, pp. 270–277.

[17] O. Benjak and D. Gerling, "Review of position estimation methods for PMSM drives without a position sensor, part III: Methods based on saliency and signal injection," in *Proc. Int. Conf. Elect. Machines Syst.*, Oct. 2010, pp. 873–878.

[18] F. M. L. De Belie, P. Sergeant, and J. A. Melkebeek, "A sensorless drive by applying test pulses without affecting the average-current samples," *IEEE Trans. Power Electron.*, vol. 25, no. 4, pp. 875–888, Apr. 2010.

[19] D. Leggate and R. J. Kerkman, "Pulse-based dead-time compensator for PWM voltage inverters," *IEEE Trans. Ind. Electron.*, vol. 44, no. 2, pp. 618–626, Apr. 1997.

[20] J. M. Guerrero, M. Leetmaa, F. Briz, A. Zamarron, and R. D. Lorenz, "Inverter nonlinearity effects in high-frequency signal-injection-based sensorless control methods," *IEEE Trans. Ind. Appl.*, vol. 41, no. 2, pp. 618–626, Mar./Apr. 2005.

[21] G. T. Shen, W. X. Yao, B. Chen, K. Wang, K. Lee, and Z. Y. Lu, "Automeasurement of the inverter output voltage delay curve to compensate for inverter nonlinearity in sensorless motor drives," *IEEE Trans. Power Electron.*, vol. 29, no. 10, pp. 5542–5553, Oct. 2014.

[22] Z. D. Zhang and L. Y. Xu, "Dead-time compensation of inverters considering snubber and parasitic capacitance," *IEEE Trans. Power Electron.*, vol. 29, no. 6, pp. 3179–3187, Jun. 2014.

[23] J. L. Chen, T. H. Liu, and C. L. Chen, "Design and implementation of a novel high-performance sensorless control system for interior permanent magnet synchronous motors," *IET Electric Power Appl.*, vol. 4, no. 4, pp. 226–240, Apr. 2010.

[24] R. Mizutani, T. Takeshita, and N. Matsui, "Current model-based sensorless drive of salient-pole PMSM at low speed and standstill," *IEEE Trans. Ind. Appl.*, vol. 34, no. 4, pp. 841–846, Jul./Aug. 1998.

[25] I. Boldea, M. C. Paicu, G. D. Andreescu, and F. Blaabjerg, "'Active flux' DTFC-SVM sensorless control of IPMSM," *IEEE Trans. Energy Convers.*, vol. 24, no. 2, pp. 314–322, Jun. 2009.

[26] J. M. Liu and Z. Q. Zhu, "Sensorless control based on third harmonic back-EMF and PLL for permanent magnet synchronous machine," in *Proc. Int. Conf. Electron. Machines Syst.*, Oct. 2013, pp. 966–971.

[27] D. Q. Guan, D. Xiao, and M. F. Rahman, "Comparison of torque control bandwidth of HF injection, SMO and FPE direct torque control IPMSMS drives," in *Proc. Australasian Univ. Power Eng. Conf.*, Sep. 2014, pp. 1–6.

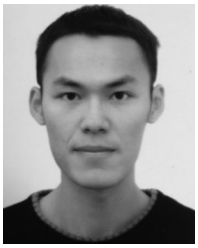

Ge Xie received the B.S. and M.S. degrees from Zhejiang University, Zhejiang, China, in 2007 and 2011, respectively. He is currently working toward the Ph.D. degree in Aalborg University, Aalborg, Denmark.

His current research interests include sensorless control of permanent-magnet synchronous machines.

Kaiyuan Lu (M'12) received the B.S. and M.S. degrees from Zhejiang University, Zhejiang, China, in 1997 and 2000, respectively, and the Ph.D. degree from Aalborg University, Aalborg, Denmark, in 2005.

In 2005, he became an Assistance Professor in the Department of Energy Technology, Aalborg University, where since 2008, he has been an Associate Professor. His current research interests include design of permanent-magnet machines, FEM analysis, and control of permanent-magnet machines.

Sanjeet Kumar Dwivedi (S'05–M'06–SM'10) received the M.Tech. degree with Gold Medal from Indian Institute of Technology (formally University of Roorkee), Roorkee, India, in 1999, and the Ph.D. degree from Indian Institute of Technology, Delhi, India, in 2006.

He joined Larsen and Toubro Ltd. as a Graduate Engineer Trainee in 1991. In 1993, he joined as a Lecturer in the Electrical Department, Government Engineering College, Sagar, India, where he became an Associate Professor in 2004 and the Head of Department in 2007. Since October 2008, he has been an R&D Engineer in the Control Engineering Department, Danfoss Power Electronics, Danfoss Drives A/S, Graasten, Denmark. His current research interests include control methods of PM motors, induction motors and synchronous reluctance motors, sensorless control of ac drives, energy-efficient control of drive, and power quality.

Dr. Dwivedi has been awarded with Merit Certificate by the Institution of Engineers India for his research publication. He is the Technical Editor of the IEEE TRANSACTIONS ON MECHATRONICS.

Jesper Riber Rosholm received the M.S. degree from Aalborg University, Aalborg, Denmark, in 1995.

In 1995, he joined Danfoss A/S, Graasten, Denmark as a Development Engineer and became the Manager of Control Engineering in Drive Division in 2007, and since 2014, he has been leading the Control Engineering Department of Danfoss Drives A/S as the Director. His current research interests include control methods of PM motors, induction motors, and synchronous reluctance motors.

Frede Blaabjerg (S'86–M'88–SM'97–F'03) received the Ph.D. degree from Aalborg University, Aalborg, Denmark, in 1992.

He is currently with Aalborg University. He was with ABB-Scandia, Randers, Denmark, from 1987 to 1988. He became an Assistant Professor in 1992, an Associate Professor in 1996, and a Full Professor of power electronics and drives in 1998. His current research interests include power electronics and its applications such as in wind turbines, PV systems, reliability, harmonics, and adjustable speed drives.

Dr. Blaabjerg has received 15 IEEE Prize Paper Awards, the IEEE PELS Distinguished Service Award in 2009, the EPE-PEMC Council Award in 2010, the IEEE William E. Newell Power Electronics Award 2014 and the Villum Kann Rasmussen Research Award 2014. He was an Editor-in-Chief of the IEEE TRANSACTIONS ON POWER ELECTRONICS from 2006 to 2012. He has been a Distinguished Lecturer for the IEEE Power Electronics Society from 2005 to 2007 and for the IEEE Industry Applications Society from 2010 to 2011. He is nominated in 2014 by Thomson Reuters to be among the most 250 cited researchers in the engineering world.